

Defect chemistry engineering of Ga-doped garnet electrolyte with high stability for solid-state lithium metal batteries

Sihan Chen(陈思汗), Jun Li(黎俊), Keke Liu(刘可可), Xiaochen Sun(孙笑晨), Jingwei Wan(万京伟), Huiyu Zhai(翟慧宇), Xinfeng Tang(唐新峰), and Gangjian Tan(谭刚健)

Citation: Chin. Phys. B, 2024, 33 (**8**): 088203. DOI: 10.1088/1674-1056/ad41b9

What follows is a list of articles you may be interested in

Accurate estimation of Li/Ni mixing degree of lithium nickel oxide cathode materials

Penghao Chen(陈鹏浩), Lei Xu(徐磊), Xiqian Yu(禹习谦), and Hong Li(李泓)

Chin. Phys. B, 2024, 33 (**5**): 058202. DOI: 10.1088/1674-1056/ad3036

Synthesis and electrochemical performance of La_2CuO_4 as a promising coating material for high voltage Li-rich layered oxide cathodes

Fuliang Guo(郭福亮), Jiaze Lu(卢嘉泽), Meihua Su(苏美华), Yue Chen(陈约), Jieyun Zheng(郑杰允), Liang Yin(尹良), and Hong Li(李泓)

Chin. Phys. B, 2023, 32 (**8**): 088201. DOI: 10.1088/1674-1056/acd2bc

A novel calculation strategy for optimized prediction of the reduction of electrochemical window at anode

Guochen Sun(孙国宸), Jian Gao(高健), and Hong Li(李泓)

Chin. Phys. B, 2023, 32 (**7**): 078201. DOI: 10.1088/1674-1056/accd51

A high-performance rechargeable Li-O_2 battery with quasi-solid-state electrolyte

Jia-Yue Peng(彭佳悦), Jie Huang(黄杰), Wen-Jun Li(李文俊), Yi Wang(王怡), Xiqian Yu(禹习谦), Yongsheng Hu(胡勇胜), Liquan Chen(陈立泉), Hong Li(李泓)

Chin. Phys. B, 2018, 27 (**7**): 078201. DOI: 10.1088/1674-1056/27/7/078201

A low cost composite quasi-solid electrolyte of LATP, TEGDME, and LiTFSI for rechargeable lithium batteries

Jie Huang(黄杰), Jia-Yue Peng(彭佳悦), Shi-Gang Ling(凌仕刚), Qi Yang(杨琪), Ji-Liang Qiu(邱纪亮), Jia-Ze Lu(卢嘉泽), Jie-Yun Zheng(郑杰允), Hong Li(李泓), Li-Quan Chen(陈立泉)

Chin. Phys. B, 2017, 26 (**6**): 068201. DOI: 10.1088/1674-1056/26/6/068201

Defect chemistry engineering of Ga-doped garnet electrolyte with high stability for solid-state lithium metal batteries

Sihan Chen(陈思汗)[1], Jun Li(黎俊)[1], Keke Liu(刘可可)[1], Xiaochen Sun(孙笑晨)[1], Jingwei Wan(万京伟)[1,2], Huiyu Zhai(翟慧宇)[1,2], Xinfeng Tang(唐新峰)[1,‡], and Gangjian Tan(谭刚健)[1,†]

[1] *State Key Laboratory of Advanced Technology for Materials Synthesis and Processing, Wuhan University of Technology, Wuhan* 430070, *China*
[2] *International School of Materials Science & Engineering, Wuhan University of Technology, Wuhan* 430070, *China*

(Received 30 January 2024; revised manuscript received 12 April 2024; accepted manuscript online 23 April 2024)

Ga-doped $Li_7La_3Zr_2O_{12}$ (Ga-LLZO) has long been considered as a promising garnet-type electrolyte candidate for all-solid-state lithium metal batteries (ASSLBs) due to its high room temperature ionic conductivity. However, the typical synthesis of Ga-LLZO is usually accompanied by the formation of undesired $LiGaO_2$ impurity phase that causes severe instability of the electrolyte in contact with molten Li metal during half/full cell assembly. In this study, we show that by simply engineering the defect chemistry of Ga-LLZO, namely, the lithium deficiency level, $LiGaO_2$ impurity phase is effectively inhibited in the final synthetic product. Consequently, defect chemistry engineered Ga-LLZO exhibits excellent electrochemical stability against lithium metal, while its high room temperature ionic conductivity ($\sim 1.9\times10^{-3}$ S·cm^{-1}) is well reserved. The assembled Li/Ga-LLZO/Li symmetric cell has a superior critical current density of 0.9 mA·cm^{-2}, and cycles stably for 500 hours at a current density of 0.3 mA·cm^{-2}. This research facilitates the potential commercial applications of high performance Ga-LLZO solid electrolytes in ASSLBs.

Keywords: Ga-doped $Li_7La_3Zr_2O_{12}$ (Ga-LLZO), defect chemistry engineering, high room temperature ionic conductivity, electrochemical stability

PACS: 82.47.Aa, 82.33.Pt, 31.15.–p, 82.45.Gj **DOI:** 10.1088/1674-1056/ad41b9

1. Introduction

With the rise of the new energy vehicle industry, breakthroughs in lithium-ion batteries[1–4] regarding high energy density and safety performance have become increasingly crucial. Currently, lithium-ion batteries employing organic liquid electrolytes have achieved significant success, and are widely used in commercial applications. However, for the demands of higher energy density, reliability, and safety, existing liquid electrolytes still exhibit notable limitations. For instance, the organic liquid electrolytes are not only flammable but incompatible with high-voltage ($\geq$ 4.6 V) cathodes or larger-capacity lithium metal anodes.[5] In this context, all-solid-state lithium metal batteries (ASSLBs) have emerged as a promising alternative, offering excellent safety features and high energy density. The solid-state electrolytes (SSEs) used in ASSLBs possess sufficient mechanical strength to prevent lithium dendrite penetration and typically have an electrochemical stability window exceeding 5 V.[6] This enables the use of lithium metal anodes and high-voltage cathode materials, which is beneficial to achieve higher energy density limits. However, SSEs, as the critical components in ASSLBs, must exhibit high stability against lithium metal.

SSEs are generally divided into three categories: inorganic ceramic electrolytes (including sulfides, halides and oxides), polymer electrolytes, and composite electrolytes. Specifically, sulfide-based electrolytes mainly include $Li_{10}GP_2S_{12}$ (LGPS), Li_2S–P_2S_5 systems, $Li_7P_3S_{11}$, and so on.[7] Halide electrolytes[8] generally fall into three categories: (i) Li_a-M-Cl_6, (ii) Li_a-M-Cl_4 and (iii) Li_aM-C_{l8} (M = transition metal elements).[9] They always show the highest Li-ion conductivity[10] (σ_{Li+}) over 10^{-3} S·cm^{-1} at room temperature. However, they are extremely sensitive to air and suffer from high industrial production costs. Oxide-based electrolytes encompass LiPON, perovskite-type, NASICON-type,[11,12] and garnet-type electrolytes.[13,14] Polymer electrolytes mainly include polyethylene oxide (PEO),[15] polyvinylidene fluoride (PVDF),[16] poly(methyl methacrylate) (PMMA),[17] polypropylene (PAN),[18] etc.[19–21] They have become popular SSEs due to their good flexibility and low cost. The latest report by Xiong[22] *et al*. reported 4.2 V polymer-based ASSLBs using high-concentration PEO solid electrolyte, providing a potential pathway for high-voltage stable polymer electrolytes in high-energy density lithium batteries. However, polymer electrolytes tend to crystallize at room temperature, resulting in a deterioration of σ_{Li+} ranging from 10^{-8} S·cm^{-1} to 10^{-6} S·cm^{-1}.[23] Besides, polymer electrolytes risk flammability, which hinders their widespread use.[24] Composite SSEs are a proportional mixture of ceramics and polymers.[25] Therefore, they combine some advantages of both ceramic and polymer SSEs, but still encounter challenges such as low room temperature σ_{Li+}, making their

†Corresponding author. E-mail: gtan@whut.edu.cn
‡Corresponding author. E-mail: tangxf@whut.edu.cn

© 2024 Chinese Physical Society and IOP Publishing Ltd

practical applications quite difficult.[26]

Oxide SSEs are currently a research hotspot for electrolyte materials due to their higher mechanical strength, good chemical stability, and high safety performance. However, oxide SSEs often suffer from severe interface contact issues, which hinders their development in full batteries. In response to this problem, various methods have been employed to modify electrolytes. A new type of solid electrolyte, receptor-doped $LiTaSiO_5$, was designed and synthesized by Wang[27] *et al*. Additionally, a zirconium-doped $LiTaSiO_5$ electrolyte, $Li_{1.1}Ta_{0.9}Zr_{0.1}SiO_5$, was successfully synthesized. Its conductivity at 25 °C is approximately 2.97×10^{-5} S·cm^{-1}, which is about two orders of magnitude higher than that of $LiTaSiO_5$. Wu[28] *et al.* has revealed the presence of one-dimensional liquid lithium ion conduction in $LiTa_2PO_8$ and its derivatives. This liquid-like conduction endows Li/$LiTa_2PO_8$/Li batteries with high ionic conductivity (1.2 mS·cm^{-1} at 30 °C) and exceptional stability. This finding provides principles for the future discovery and design of improved solid electrolytes that do not require modifications to the Li/solid electrolyte interface to achieve stable ionic transport. Recently, the garnet-type $Li_7La_3Zr_2O_{12}$ (LLZO) SSEs have attracted great attention due to their satisfactory room temperature σ_{Li+} (10^{-4}–10^{-3} S·cm^{-1}), and wide electrochemical window ($\sim$ 6 V vs. Li^+/Li) and being relatively inert to air.[29] Pristine LLZO is a tetragonal phase with the positions of tetrahedra, octahedra, and off-center octahedra being fully occupied by lithium ions, and exhibits a low room temperature σ_{Li+}, approximately $\sim 10^{-6}$ S·cm^{-1} at 25 °C.[30] By doping LLZO with Al/Ga/Fe[31–37] at Li sites, Ge/Sr/Ce[38–40] at La sites, or Ta/Nb/Ti[41–43] at Zr sites, LLZO transforms to cubic phase, and an disordered distribution of lithium is observed, creating more pathways for lithium ion migration. As such, the σ_{Li+} of cubic LLZO is two orders of magnitude higher than that of the tetragonal one.[44] In particular, Ga-doped LLZO (Ga-LLZO) exhibits outstanding room temperature σ_{Li+} of $\sim 2\times10^{-3}$ S·cm^{-1}.[45] Nonetheless, recent studies[33,46–49] suggest that Ga-LLZO displays instability issue (cracking) in contact with Li metal anode, owing to the presence of $LiGaO_2$ impurity phase in the synthetic product that has a strong reaction with Li metal.

To get rid of the undesired $LiGaO_2$ phase, researchers have tried to pre-add SiO_2 during the synthesis of Ga-LLZO.[50] It is found that $LiGaO_2$ phase is effectively inhibited from the final product by compounding with SiO_2 to form Li_2SiO_3. As a result, the stability of Ga-LLZO against Li metal is greatly improved. However, since Li_2SiO_3 is an ionic insulator, it seriously degrades the σ_{Li+} of Ga-LLZO from 2.0×10^{-3} S·cm^{-1} to 0.4×10^{-3} S·cm^{-1}. There is an urgent need to develop a new method that ensures both electrochemical stability and high σ_{Li+} of Ga-LLZO.

In this study, we demonstrate that, by intentionally introducing an appropriate amount of additional Li vacancies in Ga-LLZO, the synthetic product contains negligible amount of $LiGaO_2$ impurity phase. Our theoretical calculations reveal that Li vacancies favor the solubility of Ga in LLZO. This approach dissolves $LiGaO_2$ into Ga-LLZO without generating additional impurity phases, thus avoiding the loss of σ_{Li+}. The introduction of 1 mol% Li vacancies in Ga-LLZO not only significantly enhances its stability against Li metal but maintains high σ_{Li+} of 1.9×10^{-3} S·cm^{-1} at room temperature, enabling defect chemistry engineered Ga-LLZO a competitive solid electrolyte. The practicality of these materials in ASSLBs is further demonstrated in the assembled half-cells.

2. Experiment details

The raw materials of Li_2CO_3, Ga_2O_3, La_2O_3 and ZrO_2 were weighed according to the chemical compositions of $Li_{6.25(1-x)}Ga_{0.25}La_3Zr_2O_{12}$ ($x = 0.1\%$, 0.3%, 0.5%, 1%, 2%, 3%, 4%, 5%) and ball milled at a speed of 200 rpm for 5 hours, with ZrO_2 as the milling medium and ethanol as the solvent. After drying in an oven at 80 °C for 12 hours, the mixture is then further processed in an agate mortar to ensure the homogeneity. They were then separately loaded into crucibles and transferred into muffle furnaces, which had been preheated to 1100 °C. After reaction for 14 min, the crucibles were taken out from the furnace and cooled down to room temperature naturally in air. Finally, the samples were placed into a graphite mold with an inner diameter of 12.5 mm and a height of approximately 70 mm for hot pressing in vacuum atmosphere. Coiled carbon paper was used to separate the punches and samples from the mold. The hot-pressing procedure is described as follows: the samples were first heated to 1100 °C at a rate of 30 °C per minute under an axial pressure of 40 MPa and held there for 1 hour. Subsequently, the samples were cooled down at a rate of 10 °C per minute to obtain highly dense Ga-LLZO electrolyte pellets.

The phase purity of the synthesized electrolyte pellets was examined by powder x-ray diffraction (Empyrean, PANalytical, Holland, Cu $K\alpha$) with 2θ ranging from 10° to 80°. Microstructural studies were conducted using field-emission scanning electron microscopy (FESEM) (SU8000, Hitachi, Japan). Backscattered electron (BSE) images and elemental distribution mappings were captured using electron probe microanalysis (EPMA, JXA-8530 F Plus, JEOL, Japan).

Electrochemical impedance spectroscopy (EIS) was conducted using a BioLogic VSP-300 electrochemical workstation with an AC amplitude of 10 mV and a frequency range of 1 Hz to 7×10^6 Hz to determine the σ_{Li+} of electrolyte pellets. The VTC-16D sputter coater (Hefei Kejing group) was employed to pre-sputter thin gold layers on both sides of the electrolyte pellets as ion-blocking electrodes.

Symmetric cells of Li|Ga-LLZO|Li were assembled in a glovebox filled with ultra-pure argon to avoid lithium metal oxidation. Lithium blocks were cut into lithium disks and pressed into uniform thickness. In a typical half-cell assembly, the garnet electrolyte pellet was polished sequentially with 120, 400, 800, 2000, and 5000-grit sandpapers, followed by clamping between two new lithium disks. Subsequently, both sides underwent heat treatment at 250 °C for 30 min using a hot plate. After cooling, the prepared interlayer cell was sealed well in a coin cell (CR 2032).

Density functional theory calculations were performed using the Vienna *Ab-initio* Simulation Package (VASP).[51,52] All calculations employed the Perdew–Burke–Ernzerhof (PBE)[53] spin-polarized generalized gradient approximation functional.[53] Atomic positions were optimized by minimizing the total energy difference (less than 10^{-6} eV) and forces (less than 0.01 eV/Å). A cutoff energy of 520 eV was sufficient for the convergence of the total energy for $Li_7La_3Zr_2O_{12}$ (LLZO). A $3\times3\times3$ k-point grid was used for the supercell of $1\times1\times1$ Ga-LLZO following the Monkhorst–Pack scheme.

To elucidate the influence of lithium vacancies (V_{Li}) on the formation energy of Ga substitution for Li (Ga_{Li}) defects, the defect formation energy (E_{df}) was calculated using the following formula:

$$E_{df} = E_1 - E_0 - n\mu. \tag{1}$$

Here, E_1 represents the formation energy of defective Ga-LLZO, E_0 represents the formation energy of pristine Ga-LLZO, n is the number of defective atoms, and μ is the chemical potential of the defective atoms.

3. Results and discussion

3.1. Inhibiting $LiGaO_2$ from Ga-LLZO by engineering Li vacancies

First-principles theoretical calculations are employed to elucidate why $LiGaO_2$ forms and how to inhibit it from Ga-LLZO by defect chemistry engineering. As shown in Fig. 1, the defect formation energy (E_{df}) of Ga substitution for Li (Ga_{Li}) in LLZO is constantly a large positive value over a wide range of Fermi energy (E_f). This indicates that Ga hardly substitutes Li so that it easily precipitates out as $LiGaO_2$ impurity phase. E_{df} of Ga_{Li} is remarkably decreased in the presence of Li vacancies (V_{Li}), although it is still positive. More importantly, E_{df} of Ga_{Li} would become even lower if more V_{Li} is introduced, i.e., the E_{df} of ($Ga_{Li}+2V_{Li}$, $2V_{Li}$:2Li vacancies) is far below that of ($Ga_{Li}+1V_{Li}$, $1V_{Li}$:1Li vacancie). In this context, we argue that the employment of Li vacancies in LLZO is beneficial to form Ga_{Li} substitutional defects rather than $LiGaO_2$ impurities. This defect chemistry engineering approach (through introducing an appropriate amount of Li vacancies) enables the synthesis of phase pure Ga-LLZO electrolyte without generating additional impurities (such as ionic insulating Li_2SiO_3 being transformed from $LiGaO_2$ by adding SiO_2).[50] Therefore, superior electrochemical performance is expected in this work with respect to previous studies,[50] as will be discussed below.

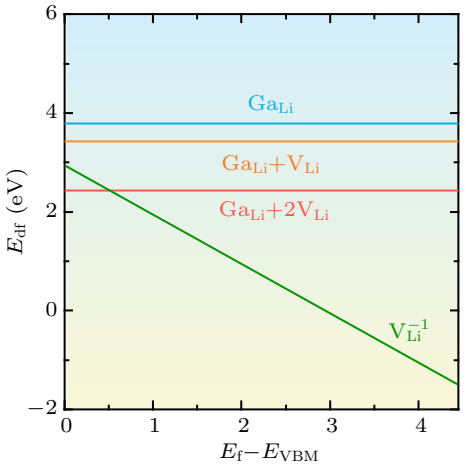


Fig. 1. The formation energy of various defects in Ga-LLZO with respect to ($E_f - E_{VBM}$). E_{VBM} is the energy of valence band maxima.

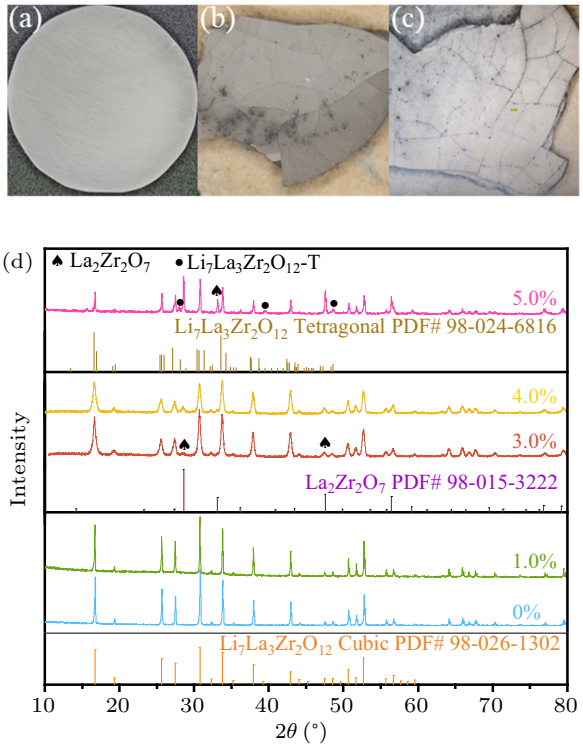


Fig. 2. Photographs of Ga-LLZO pellets with different values of x after hot pressing: (a) $x=3\%$, (b) $x=4\%$ and (c) $x=5\%$. (d) XRD patterns for several representative samples. The standard diffraction patterns of $La_2Zr_2O_7$ (PDF card #98-015-3222), cubic $Li_7La_3Zr_2O_{12}$ (PDF card #98-026-1302) and tetragonal $Li_7La_3Zr_2O_{12}$ (PDF card #98-024-6816) are depicted for reference.

Figures 2(a)–2(c) show photographs of Ga-LLZO pellets with different amounts of additional Li vacancies (3%, 4%, and 5% in mole fractions, respectively) after hot pressing. Apparently, in pellets with $x \leq 3\%$ no cracks are observed. How-

ever, as $x \geq 4\%$, the pellets become fragmentary, probably attributing to the presence of $La_2Zr_2O_7$ impurity phase (see discussions below) that causes substantial internal stress within the grain boundaries.[54]

Figure 2(d) displays the powder x-ray diffraction (XRD) patterns of several representative Ga-LLZO pellets. Samples with $x \leq 1\%$ are pure phase compounds crystallizing in cubic garnet structure. As x is increased to 3%, $La_2Zr_2O_7$ impurities appear. Moreover, the increasing Li vacancies in $x = 3\%$ and 4% samples make them more defective (in a metastable state), leading to accumulated internal stress that broadens diffraction patterns. In the $x = 5\%$ sample, the huge internal stress gets released by structure collapse partially into tetragonal phase, and the XRD patterns get intensified again. A previous study by Paolella[55] *et al.* suggests that the stabilization of cubic LLZO phase via controlling Li loss is rather complex. In the absence of foreign dopants, the vacancies in Li-sites facilitate the formation of cubic LLZO. However, the Li-deficient LLZO is only stable at high temperatures, and it recovers to tetragonal phase once cooling to room temperature. In the case of aggressive Li loss, the synthetic products include lithium-deficient LLZO unstable phase (tetragonal) or off-stoichiometric LLZO or pyrochlore ($La_2Zr_2O_7$), which is consistent with our study. In the same study, the authors also demonstrate that Ga dopant makes Li loss more controllable to form stabilized cubic LLZO. Therefore, we conjecture that Ga dopant predominately contributes to the stabilization of cubic LLZO in this study rather than Li vacancies. In this context, excess Li vacancies are supposed to destabilize cubic Ga-doped LLZO and lead to the formation of tetragonal phase ($x = 3\%$–4%) and even $La_2Zr_2O_7$ ($x = 5\%$).

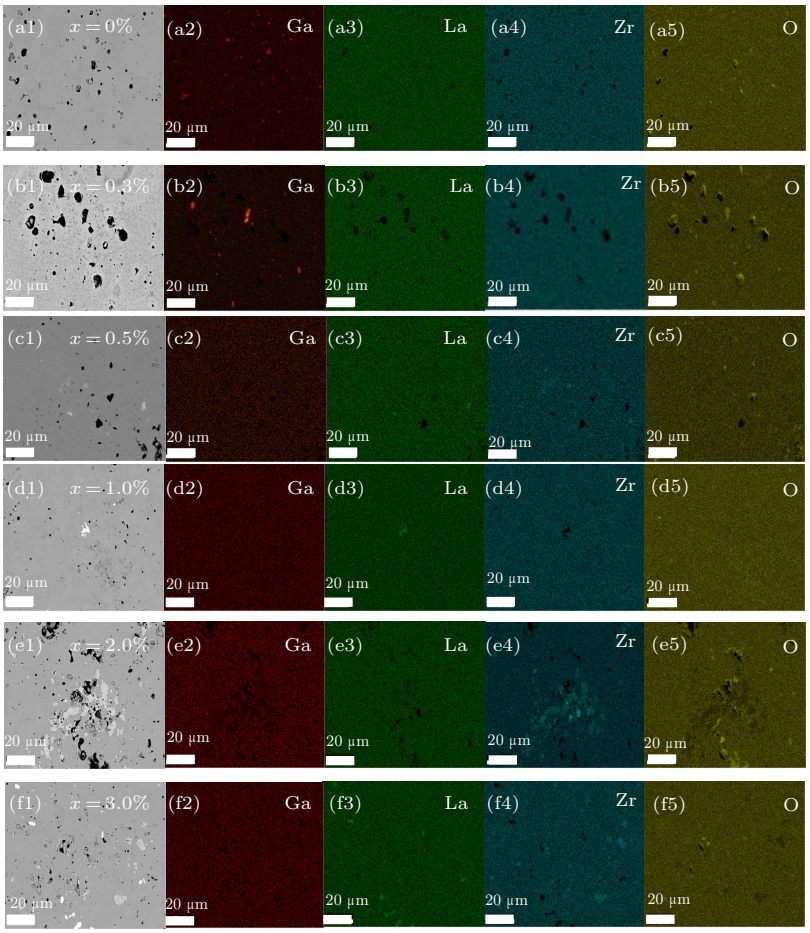


Fig. 3. (a)–(f) The backscattered electron images and elemental distribution mappings of (a2)–(f2) Ga, (a3)–(f3) La, (a4)–(f4) Zr and (a5)–(f5) O for Ga-LLZO pellets with $x \leq 3\%$.

Figures 3(a1)–3(f1) show the BSE images of Ga-LLZO with $x = 0$, 0.3%, 0.5%, 1.0%, 2.0% and 3.0%, respectively. The corresponding elemental distribution mappings of Ga, La, Zr and O are presented in Figs. 3(a2)–3(f2), 3(a3)–3(f3), 3(a4)–3(f4) and 3(a5)–3(f5), respectively. In the $x = 0$ sample, a conspicuous Ga aggregation phenomenon (Fig. 3(a2)) is observed. Previous TEM results corroborate that these Ga-rich precipitates in EDS represent $LiGaO_2$.[50] Therefore, we can ascertain that the observed Ga enrichment in the $x = 0\%$ (Fig. 3(a2)) and $x = 0.3\%$ (Fig. 3(b2)) samples is attributed to the presence of the $LiGaO_2$ impurity phase (although undetectable in XRD studies because of its low concentration).

Ga-rich precipitates become much sparser in Li-deficient samples and basically vanish when $x \geq 0.5\%$ (Figs. 3(c2)–3(f2)). In the meanwhile, Zr-rich impurities (most likely $La_2Zr_2O_7$ according to XRD analysis) are prone to precipitae out, and it becomes evident when $x = 2\%$ (Fig. 3(e4)). The presence of $La_2Zr_2O_7$ is further supported by the point scanned EDS analysis (Fig. S1).

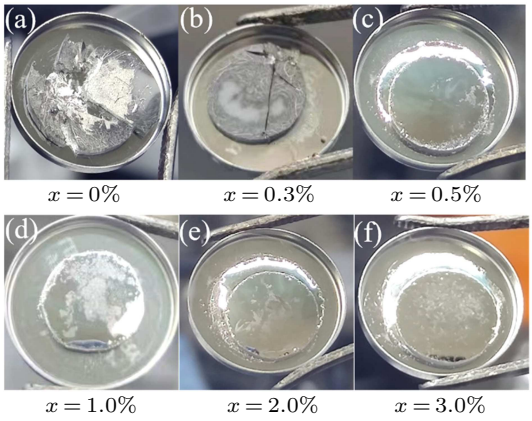


Fig. 4. Photographs of Ga-LLZO pellets with different Li vacancies after being immersed in molten lithium for 1 min: (a) $x = 0$, (b) $x = 0.3\%$, (c) $x = 0.5\%$, (d) $x = 1\%$, (e) $x = 2\%$ and (f) $x = 3\%$.

The inhibition of $LiGaO_2$ in Ga-LLZO final product by Li deficiency significantly improves its stability against Li metal. Figure 4 illustrates the photographs of Ga-LLZO pellets with different Li vacancies ($x \leq 3\%$) after being immersed in molten lithium for 1 min. The $x = 0\%$ sample (Fig. 4(a)) is completely destroyed into small fragments, which is ascribed to the severe reaction between $LiGaO_2$ impurities and Li metal causing huge volume expansion and stress release. By comparison, the $x = 0.3\%$ sample (Fig. 4(b)) containing less $LiGaO_2$ preserves structural integrity, although several cracks radiating from the center of the pellet are observed. For the samples with $x \geq 0.5\%$ (Figs. 4(c)–4(f)), they remain intact after immersion because of absence of $LiGaO_2$ precipitates.

3.2. Superior electrochemical performance of defects engineered Ga-LLZO

Figure 5(a) displays the EIS of Ga-LLZO pellets with different content of additional Li vacancies, from which their room temperature values of σ_{Li+} are determined, as illustrated in Fig. 5(b). It is seen that σ_{Li+} is practically unaffected within $x \leq 3\%$, roughly scattering around 2×10^{-3} S·cm^{-1}. As x is increased to 4% and above, there is a rapid decline of σ_{Li+} to a value as low as 0.1×10^{-3} S·cm^{-1}, because of the emergence of poor-ionic-conductive $La_2Zr_2O_7$ impurity phase and collapse of cubic garnet structure into tetragonal one[54] (in the circumstance of over-much Li deficiency).

Ideal electrolytes[56] are not only highly ionic conductive but also electrically insulating. Figure 5(c) shows direct current (DC) polarization curves for Ga-LLZO pellets investigated in this study. The derived electronic conductivity (σ_e) values are all on the order of 10^{-6} mS·cm^{-1} (six orders of magnitude lower than those of σ_{Li+}) at 25 °C, regardless of x, as shown in Fig. 5(d). Therefore, our defects engineered Ga-LLZO can be viewed as excellent electronic insulator so that short circuits or electrical leakages can be largely inhibited during their service in batteries.

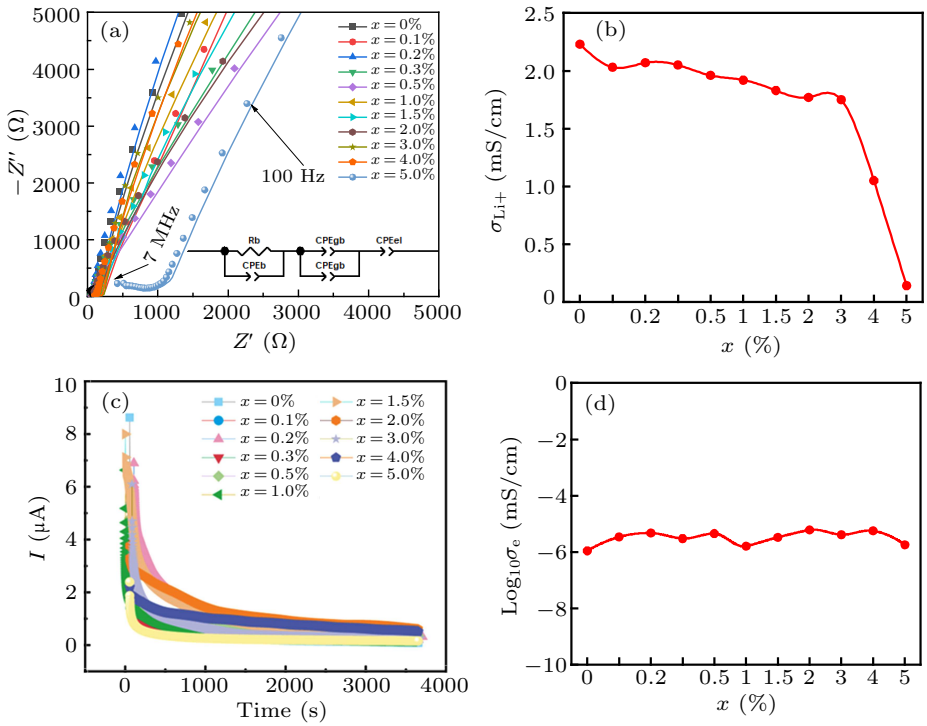


Fig. 5. (a) EIS curves and their equivalent circuits, (b) σ_{Li+}, (c) DC polarization curves, and (d) σ_e for Ga-LLZO pellets with varying Li vacancies. Insets of (a) and (c) are illustrations of equivalent circuits.

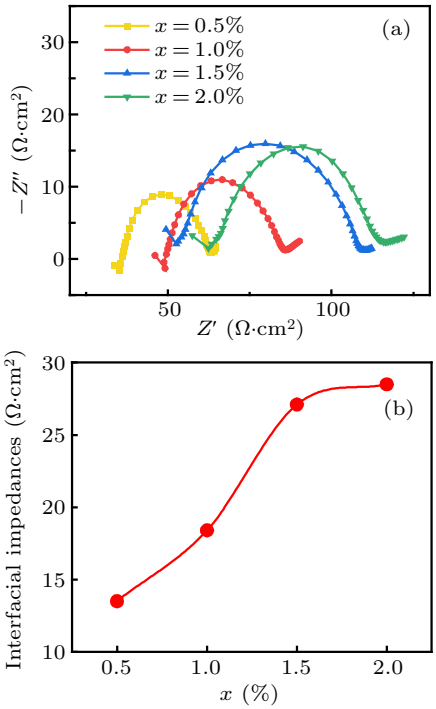


Fig. 6. (a) EIS curves of Li|Ga-LLZO|Li symmetric cells with x in-between 0.5% and 2%. (b) Interfacial impedances of Li|Ga-LLZO|Li symmetric cells with x in-between 0.5% and 2%.

Li|Ga-LLZO|Li symmetric cells were successfully assembled for the electrolyte pellets with x in-between 0.5% and 2% where $LiGaO_2$ or $La_2Zr_2O_7$ impurities are absent. Figure 6(a) illustrates the EIS curves of these cells, from which the interfacial impedances (Fig. 6(b)) are estimated to be 13.5 Ω·cm^2 ($x = 0.5\%$) and 18.4 Ω·cm^2 ($x = 1\%$), respectively. These values are among the best results[46,49,50,57–59] reported so far for garnet electrolytes based symmetric cells, which is indicative of satisfactory interfacial contact. However, the interfacial impedances are almost doubled at ∼ 28 Ω·cm^2 when x is 1.5% or larger (Fig. 6(b)). Although these values are still decent, they indicate lower priority for the over-much-Li-deficient electrolytes in battery assembly.

The cyclic current curves shown in Fig. 7 demonstrate that the symmetric cells with $x = 0.5\%$, 1%, 1.5% and 2% do not short circuit until high critical current densities (CCD) of 0.9 mA cm^{-2}, 1.0 mA·cm^{-2}, 0.9 mA·cm^{-2} and 0.7 mA·cm^{-2} are achieved, respectively. Although $x = 2\%$ sample does not contain $LiGaO_2$, it has a tremendous amount of $La_2Zr_2O_7$ impurities (see Figs. 3(e1)–3(e5)). As $La_2Zr_2O_7$ is a poor ionic conductor, it is very likely to exert an adverse impact on the electrochemical performance of the pellet. Therefore, the $x = 2\%$ sample shows a degraded CCD compared to other three samples shown in Fig. 7.

The best performing Li|Ga-LLZO|Li symmetric cell with $x = 1\%$ was further subjected to long-term cycles. In an applied current density of 0.1 mA·cm^{-2}, the cell stably cycles for over 500 hours (Fig. S2). We then proceed to increase the current density to 0.3 mA·cm^{-2}, and the results are displayed in Fig. 8(a). Figures 8(b)–8(d) illustrate the magnified voltage profiles of the symmetric cell in the three representative regions (I, II and III, respectively) marked by the blue-dashed rectangles in Fig. 8(a). Apparently, the voltage platform is fairly flat after cycling for 260 hours, which is encouraging. The cell, however, suffers a micro-short circuit during the 449th hour cycling and this situation becomes even worse after cycling for 470 hours, as can be seen from the sudden drop in voltages. Nonetheless, we demonstrate the defects engineered Ga-LLZO pellet has good compatibility with Li metal anode and practicability in ASSLBs because of its well reserved σ_{Li+} of 1.9×10^{-3} S·cm^{-1} and much improved stability. The excellent cycling performance also indicates the electrolyte's inhibition effect on lithium dendrites, as suggested by Wu *et al.*[60] Our findings hold significant implications for ongoing studies of electrolyte-electrode stability in ASSLBs.

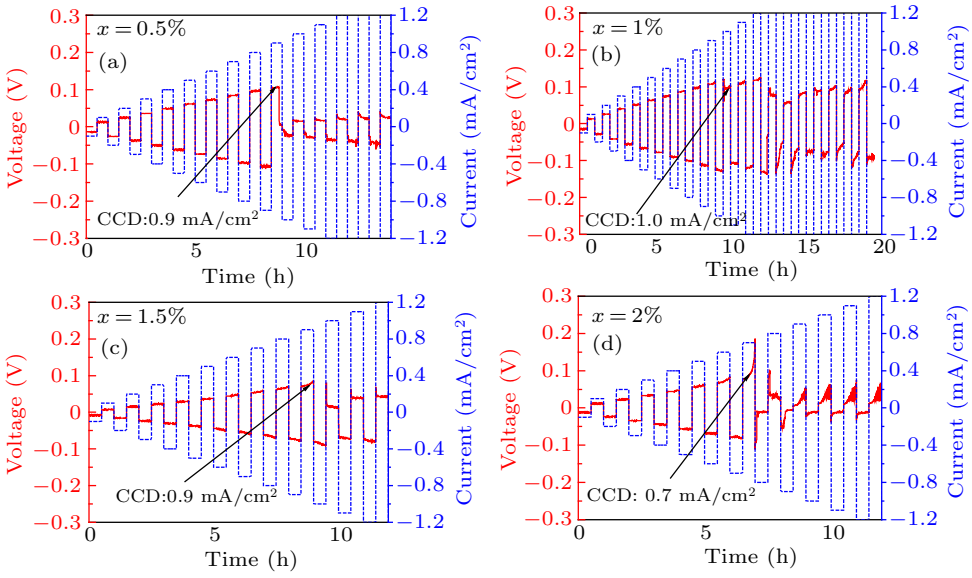


Fig. 7. Critical current density test of the Li|Ga-LLZO|Li symmetric cells with (a) $x = 0.5\%$, (b) $x = 1\%$, (c) $x = 1.5\%$, and (d) $x = 2\%$.

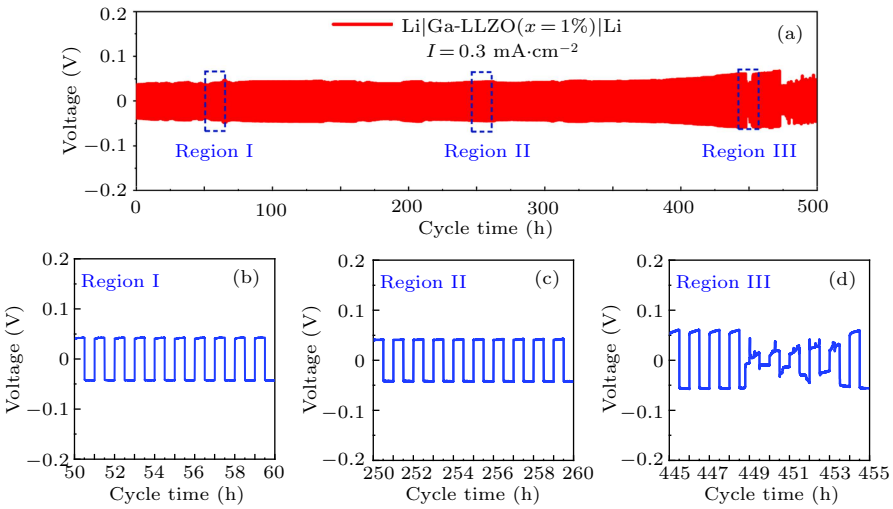


Fig. 8. (a) Galvanostatic cycling performance of Li|Ga-LLZO|Li symmetric cells with $x = 1\%$ operating at a current density of 0.3 mA·cm^{-2}. The blue-dashed rectangles are three representative regions (I, II and III). The magnified voltage profiles from (b) 50 h to 60 h (region I), (c) 250 h to 260 h (region II), and (d) 445 h to 455 h (region III).

4. Conclusion

Ga-LLZO was regarded as a promising electrolyte candidate for ASSLBs but encounters an instability issue in contact with a Li metal anode. The spontaneously formed $LiGaO_2$ impurity phase in the synthetic product of Ga-LLZO (due to the inherently low solubility of Ga in LLZO) has a vigorous reaction with Li metal, resulting in a huge volume change and stress release that crack the electrolyte pellet. Although researchers have successfully transformed the undesired $LiGaO_2$ impurities into Li_2SiO_3 byproducts (which are stable against Li metal) by pre-adding SiO_2 in the synthesis procedure and improved the stability of Ga-LLZO, the ionically insulating Li_2SiO_3 has a negative impact on the overall σ_{Li+} of electrolyte pellet. In this work, we employed a feasible defect chemistry engineering approach to inhibit $LiGaO_2$ impurities from the final product of Ga-LLZO. Specifically, we reveal that the introduction of additional Li vacancies in LLZO significantly reduces the Ga_{Li} substitutional defects formation energy, so that $LiGaO_2$ impurities are able to be redissolved into the garnet electrolyte. This defect chemistry engineering approach ensures a high σ_{Li+} of 1.9×10^{-3} S·cm^{-1}, low σ_e on the order of 10^{-6} mS·cm^{-1}, and a large CCD of 1.0 mA·cm^{-2} for $LiGaO_2$-free Ga-LLZO electrolyte pellets that show excellent stability against Li metal model. The assembled Li|Ga-LLZO|Li symmetric cells display satisfactory long cycling performance.

Acknowledgements

This work was financially supported by the National Natural Science Foundation of China (Grant No. 52171221) and the National Key Research and Development Program of China (Grant No. 2019YFA0704900).

References

[1] Wang X, Jing T and Liang D 2023 *Chin. Phys. B* **32** 067102
[2] Wang L, Li N, Chen H S and Song W L 2023 *Chin. Phys. B* **32** 108201
[3] Chen F, Lin J, Chen Y, Dong B, Yin C, Tian S, Sun D, Xie J, Zhang Z and Li H 2022 *Chin. Phys. B* **31** 058101
[4] Chen F, Zeng C, Huang C, Lin J, Chen Y, Dong B, Yin C, Tian S, Sun D and Zhang Z 2022 *Chin. Phys. B* **31** 078101
[5] Kalhoff J, Eshetu G G, Bresser D and Passerini S 2015 *ChemSusChem* **8** 2154
[6] Thangadurai V and Weppner W 2005 *Adv. Funct. Mater.* **15** 107
[7] Kamaya N, Homma K, Yamakawa Y, Hirayama M, Kanno R, Yonemura M, Kamiyama T, Kato Y, Hama S and Kawamoto K 2011 *Nat. Mater.* **10** 682
[8] Nie X, Hu J and Li C 2023 *Interdiscip. Mater.* **2** 365
[9] Lutz H, Kuske P and Wussow K 1987 *Z. Anorg. Allg. Chem.* **553** 172
[10] Asano T, Sakai A, Ouchi S, Sakaida M, Miyazaki A and Hasegawa S 2018 *Adv. Mater.* **30** 1803075
[11] Zhang L, Liu Y, You Y, Vinu A and Mai L 2023 *Interdiscip. Mater.* **2** 91
[12] Li C, Li R, Liu K, Si R, Zhang Z and Hu Y S 2022 *Interdiscip. Mater.* **1** 396
[13] Li Y, Xu H, Chien P H, Wu N, Xin S, Xue L, Park K, Hu Y Y and Goodenough J B 2018 *Angew. Chem. Int. Ed.* **57** 8587
[14] Schnell J, Tietz F, Singer C, Hofer A, Billot N and Reinhart G 2019 *Energy Environ. Sci.* **12** 1818
[15] Xue Z, He D and Xie X 2015 *J. Mater. Chem. A* **3** 19218
[16] Jiang Z, Carroll B and Abraham K 1997 *Electrochim. Acta* **42** 2667
[17] Ali U, Karim K J B A and Buang N A 2015 *Polym. Rev.* **55** 678
[18] Zhang J, Zhao J, Yue L, Wang Q, Chai J, Liu Z, Zhou X, Li H, Guo Y and Cui G J A E M 2015 *Adv. Energy Mater.* **5** 1501082
[19] Croce F, Appetecchi G, Persi L and Scrosati B 1998 *Nature* **394** 456
[20] Wang L, Shi H, Xie Y and Wu Z S 2023 *Interdiscip. Mater.* **2** 789
[21] Xiao G, Xu H, Bai C, Liu M and He Y B 2023 *Interdiscip. Mater.* **2** 609
[22] Xiong Z, Wang Z, Zhou W, Liu Q, Wu J F, Liu T H, Xu C and Liu J 2023 *Energy Storage Mater.* **57** 171
[23] Berthier C, Gorecki W, Minier M, Armand M, Chabagno J and Rigaud P 1983 *Solid State Ionics* **11** 91
[24] Han L, Wang L, Chen Z, Kan Y, Hu Y, Zhang H and He X 2023 *Adv. Funct. Mater.* **33** 2300892
[25] Liao W and Liu C 2021 *ChemNanoMat* **7** 1177
[26] Lv F, Wang Z, Shi L, Zhu J, Edström K, Mindemark J and Yuan S 2019 *J. Power Sources* **441** 227175
[27] Wang Q, Wu J F, Lu Z, Ciucci F, Pang W K and Guo X 2019 *Adv. Funct. Mater.* **29** 1904232
[28] Wu J F, Zou Z, Pu B, Ladenstein L, Lin S, Xie W, Li S, He B, Fan Y and Pang W K 2023 *Adv. Mater.* **35** 2303730

[29] Hofstetter K, Samson A J, Narayanan S and Thangadurai V 2018 *J. Power Sources* **390** 297
[30] Buschmann H, Dölle J, Berendts S, Kuhn A, Bottke P, Wilkening M, Heitjans P, Senyshyn A, Ehrenberg H and Lotnyk A 2011 *Phys. Chem. Chem. Phys.* **13** 19378
[31] Rettenwander D, Wagner R, Langer J, Maier M E, Wilkening M and Amthauer G 2016 *Eur. J. Mineral.* **28** 619
[32] Pfenninger R, Afyon S, Garbayo I, Struzik M and Rupp J L 2018 *Adv. Funct. Mater.* **28** 1800879
[33] Wolfenstine J, Ratchford J, Rangasamy E, Sakamoto J and Allen J L 2012 *Mater. Chem. Phys.* **134** 571
[34] Xia W, Xu B, Duan H, Guo Y, Kang H, Li H and Liu H 2016 *ACS Appl. Mater. Interfaces* **8** 5335
[35] Rettenwander D, Geiger C A and Amthauer G 2013 *Inorg. Chem.* **52** 8005
[36] Kim J H, Park D H, Jang J S, Shin J H, Kim M C, Kim S B, Moon S H, Lee S N and Park K W 2022 *Chem. Eng. J.* **446** 137035
[37] Wagner R, Redhammer G n J, Rettenwander D, Senyshyn A, Schmidt W, Wilkening M and Amthauer G 2016 *Chem. Mater.* **28** 1861
[38] Dumon A, Huang M, Shen Y and Nan C W 2013 *Solid State Ionics* **243** 36
[39] Huang M, Xu W, Shen Y, Lin Y H and Nan C W 2014 *Electrochim. Acta* **115** 581
[40] Rangasamy E, Wolfenstine J, Allen J and Sakamoto J 2013 *J. Power Sources* **230** 261
[41] Gao Z, Bai Y, Fu H, Yang J, Ferber T, Feng J, Jaegermann W and Huang Y 2022 *Adv. Funct. Mater.* **32** 2112113
[42] Tang Y, Luo Z, Liu T, Liu P, Li Z and Lu A 2017 *Ceram. Int.* **43** 11879
[43] Gao J, Zhu J, Li X, Li J, Guo X, Li H and Zhou W 2021 *Adv. Funct. Mater.* **31** 2001918
[44] Awaka J, Takashima A, Kataoka K, Kijima N, Idemoto Y and Akimoto J 2011 *Chem. Lett.* **40** 60
[45] Li J, Zhang J, Zhai H, Tang X and Tan G 2022 *J. Eur. Ceram. Soc.* **42** 1568
[46] Su J, Huang X, Song Z, Xiu T, Badding M E, Jin J and Wen Z 2019 *Ceram. Int.* **45** 14991
[47] El Shinawi H and Janek J 2013 *J. Power Sources* **225** 13
[48] Huang L H and Li C C 2023 *J. Power Sources* **556** 232527
[49] Wu J F, Chen E Y, Yu Y, Liu L, Wu Y, Pang W K, Peterson V K and Guo X 2017 *ACS Appl. Mater. Interfaces* **9** 1542
[50] Li J, Luo H, Liu K, Zhang J, Zhai H, Su X, Wu J, Tang X and Tan G 2023 *ACS Appl. Mater. Interfaces* **15** 7165
[51] Kresse G and Joubert D 1999 *Phys. Rev. B* **59** 1758
[52] Kresse G and Furthmüller J 1996 *Phys. Rev. B* **54** 11169
[53] Perdew J P, Burke K and Ernzerhof M 1996 *Phys. Rev. Lett.* **77** 3865
[54] Kobi S and Mukhopadhyay A 2018 *J. Eur. Ceram. Soc.* **38** 4707
[55] Paolella A, Zhu W, Bertoni G, Savoie S, Feng Z, Demers H, Gariepy V, Girard G, Rivard E and Delaporte N 2020 *ACS Appl. Energy Mater.* **3** 3415
[56] Goodenough J B 1997 *Solid State Ionics* **94** 17
[57] Matsuda Y, Sakaida A, Sugimoto K, Mori D, Takeda Y, Yamamoto O and Imanishi N 2017 *Solid State Ionics* **311** 69
[58] Rettenwander D, Redhammer G n, Preishuber-Pflügl F, Cheng L, Miara L, Wagner R, Welzl A, Suard E, Doeff M M and Wilkening M 2016 *Chem. Mater.* **28** 2384
[59] Qin S, Zhu X, Jiang Y, Ling M e, Hu Z and Zhu J 2018 *Funct. Mater. Lett.* **11** 1850029
[60] Wu J F, Pu B W, Wang D, Shi S Q, Zhao N, Guo X and Guo X 2018 *ACS Appl. Mater. Interfaces* **11** 898